

Nanoscale

Identifying biochemical constituents involved in the mycosynthesis of zinc oxide nanoparticles

Journal:	Nanoscale
Manuscript ID	NR-ART-02-2024-000624.R1
Article Type:	Paper
Date Submitted by the Author:	04-Apr-2024
Complete List of Authors:	Brady, Nathan; Sandia National Laboratories, Center for Integrated Nanotechnologies O'Leary, Shamus; Los Alamos National Laboratory Kuo, Winson; Los Alamos National Laboratory Blackwell, Brett; Los Alamos National Laboratory, Mass Spectrometry Center for Integrated 'Omics Mach, Phillip; Los Alamos National Laboratory, Mass Spectrometry Center for Integrated 'Omics Watt, John; Los Alamos National Laboratory, Bachand, George; Sandia National Laboratories

SCHOLARONE™ Manuscripts Page 1 of 22 Nanoscale

Identifying biochemical constituents involved in the mycosynthesis of zinc oxide nanoparticles

Nathan G. Brady, Shamus L. O'Leary, Winson Kuo, Brett R. Blackwell, Philip M. Mach, John Watt, and George D. Bachand*

* Correspondence: George Bachand, gdbacha@sandia.gov

N. G. Brady, S. L. O'Leary, G. D. Bachand Center for Integrated Nanotechnologies Sandia National Laboratories Albuquerque, NM 87185, USA Email: gdbacha@sandia.gov

W. Kuo, J. Watt Center for Integrated Nanotechnologies Los Alamos National Laboratory Los Alamos, NM 87545, USA

B. R. Blackwell, P. M. Mach Mass Spectrometry Center for Integrated 'Omics Los Alamos National Laboratory Los Alamos, NM 87545, USA

Keywords: mycosynthesis, zinc oxide nanoparticles, fungal exudate, nanoparticle biosynthesis, metabolomics, proteomics

Nanoscale Page 2 of 22

Abstract

Filamentous fungi are known to secrete biochemicals that drive the synthesis of nanoparticles (NPs) that vary in composition, size, and shape; a process deemed mycosynthesis. Following the introduction of precursor salts directly to the fungal mycelia or their exudates, mycosynthesis proceeds at ambient temperature and pressure, and near neutral pH, presenting significant energy and cost savings over traditional chemical or physical approaches. The mycosynthesis of zinc oxide (ZnO) NPs by various fungi exhibited a species dependent morphological preference for the resulting NPs, suggesting that key differences in the biochemical makeup of their individual exudates may regulate the controlled nucleation and growth of these different morphologies. Metabolomics and proteomics of the various fungal exudates suggest that metal chelators, such as hexamethylenetetramine, present in high concentrations in exudates of Aspergillus versicolor are critical for the production dense, well-formed, spheroid nanoparticles. The results also corroborate that the proteinaceous material in the production of ZnO NPs serves as a surface modifier, or protein corona, preventing excessive coagulation of the NPs. Collectively, these findings suggest that NP morphology is regulated by the small molecule metabolites, and not proteins, present in fungal exudates, establishing a deeper understanding of the factors and mechanism underlying mycosynthesis of NPs.

Page 3 of 22 Nanoscale

Introduction

Nanomaterials are defined as structures with at least one dimension less than or equal to 100 nm in size, where emergent and useful phenomena arise due to their intrinsic dimensionality that are distinct from the bulk material.^{1, 2} These unique characteristics manifest as changes in the electronic, magnetic, and optical signatures, as well as enhanced antimicrobial and antiviral activity.^{2, 3} As an example, zinc oxide (ZnO) has become one of the most manufactured and studied nanomaterials due to its wide applicability in various fields, including: photovoltaics, photocatalysis, sensing, environmental remediation, drug delivery, cell imaging, and cancer therapy, to name a few.^{1, 4} Adding to its attractiveness in the biomedical realm, ZnO is non-toxic to humans, being one of five Zn compounds generally regarded as safe by the U. S. Food and Drug Administration.^{1, 5} Consequently, the worldwide production of ZnO nanoparticles (NPs) was estimated to be ~34,000 tons per year in 2022.⁶

Numerous physical (top-down) and chemical (bottom-up) approaches to NP synthesis have been applied for the synthesis of ZnO and other NPs. The former, however, tends to be energy intensive, while the latter often requires the use of toxic reducing agents, and/or non-aqueous organic solutions, impacting their biomedical potential. Both of these conventional approaches also require extreme conditions with regard to temperature, pressure, or pH, presenting barriers in the areas of energy consumption, cost, and environmental toxicity. Consequently, research into the biosynthesis of NPs as an environmentally benign alternative have risen exponentially over the last twenty years, with publications on the topic increasing from less than five per year at the beginning of the century and peaking at over 600 in 2019. In these works, various biological entities have been shown to possess the ability to create NPs, including: bacteria, yeast, plant extracts, algae, viruses, and fungi. Among these organisms, fungi have gained interest due to their ease of culture and expeditious growth in the laboratory, high metal tolerance and bioaccumulation ability, as well as the high levels of biomolecules present in their exudates, which have been hypothesized to drive NP synthesis.

While the mechanism by which fungi produce NPs is not fully understood, there is mounting evidence to support the hypothesis that secretions of metal binding peptides, small molecule metabolites, and proteins are induced by metal stress and are directly involved in the nucleation, capping, and stabilization of crystalline metal NPs.¹⁷⁻²⁰ This process may be broadly categorized as biomineralization, where soluble, biologically available metal cations are transformed into insoluble crystals. Underscoring the utility of fungi for this process, they produce a large amount of biomolecules compared to bacteria, making the conversion of metal salts into NPs very fast.²¹ Certain fungi, such as *Fusarium oxysporium* Schlecht. emend. Snyder & Hansen, also are able to produce redox enzymes that reduce metal salts to produce NPs, such as in the case of silver and gold NPs.^{19, 21-24} It should be noted here, however, that Zn does not

Nanoscale Page 4 of 22

require reduction to form ZnO NPs, as it retains a divalent charge within the lattice, so in our case secreted enzymes may only act as additional proteinaceous capping agents.

Previously, we reported a morphological dependency exhibited by five fungi when producing ZnO NPs.²⁵ In this former work, Aspergillus versicolor (Vuillemin) Tiraboschi was identified as the most prominent producer of well-defined ZnO NPs, while Cladosporium cladosporioides (Fresen.) de Vries was identified as the primary producer of a square plate morphology. Based on this observation, we hypothesized that the biochemical constituents responsible for regulating morphology could be identified by evaluating compositional differences in the biomolecules present in the respective exudates. Here, we characterized the profiles of small molecules and proteins secreted by all five previously investigated fungi using shotgun metabolomics and proteomics. Comparisons among these profiles identified constituents present in high levels in the exudate of A. versicolor that may drive the formation of the well-defined NP morphology. 16 We also investigated the effect of the metal challenge on the mycosynthesis process by probing for differences in the resulting ZnO material with and without introducing metal to the mycelia, further elucidating the main components responsible for the controlled nucleation and growth of ZnO NPs within this system. Overall, our work suggests that small molecule metabolites present in fungal exudates play a key role in the mycosynthesis of well-defined NPs, while the composition and concentration of proteins is less important.

Results and Discussion

Our approach involved using mass spectrometry-based metabolomics and proteomics to characterize the profiles of small molecules and proteins, respectively, present in the exudates of the previously investigated fungi; Aspergillus niger van Tieghem, Aspergillus versicolor (Vuillemin) Tiraboschi, Cladosporium cladosporioides (Fresen.) de Vries, Paecilomyces variotii Bainier, and Penicillium chrysogenum Thom. The composition of the fungal exudates was characterized following a "challenge" with 1 mM ZnCl₂, defined here as incubating mature fungal mycelia in a solution of Zn salt and lacking any sources of carbon or nitrogen. This condition was selected because metal stress can stimulate the secretion of biomolecules in various fungal species.^{26, 27} As such, we hypothesized that the metabolites and proteins secreted by these fungi in response to the Zn challenge would correlate with the different of morphologies of ZnO NPs. Based on prior reports, proteinaceous material can reduce metal ions to their elemental form, ²⁸ and/or form a protein corona around the forming nanoparticles (protective colloid), preventing coagulation into macroscopic structures.^{23, 29} For ZnO NPs, the catalytic potential of reductase enzymes is likely irrelevant as the Zn atoms retain a divalent charge. This supposition is consistent with prior work where the use of boiled biological exudates containing denatured and deactivated proteins resulted in higher yields of ZnO NPs.²⁹

Page 5 of 22 Nanoscale

Thus, the proteomic work in the current study focused on reporting the fungal proteomes in a discovery fashion, to serve as a signpost for future investigations. Here, all proteins identified in each of the five fungal exudates are listed in Tables S1 – S5 along with their associated accession numbers, percent coverage of the overall protein sequence encompassed by the captured fragment, and number of peptides detected. As this approach is strictly qualitative, the proteins are listed in alphabetical order, rather than ranked by quantity. A total of 312 distinct protein fragments were identified across all five fungi with *A. niger* and *C. cladosporioides* producing the greatest (189) and least (7) number of protein fragments, respectively.

To compare the proteomes across the five fungi, all uncharacterized proteins or contigs were removed from the list and the remaining 238 protein fragments were listed in Table S6 with similar proteins across fungal exudates highlighted in yellow. Interesting proteins included in both *Aspergillus* species Zn(II)2Cys6 transcription factor and Zn(2)-C6 fungal-type DNA-binding domain. These proteins contain a cystine-rich motif located at the N-terminus that is involved in Zn-dependent DNA binding,³⁰ whereby two Zn atoms are coordinated by six cysteine residues.³¹ A wide range of proteins contain this domain, including several proteins involved in the metabolism of various amino acids, catabolism of GABA and biosynthesis of leucine amino acids.³⁰⁻³² The *Aspergillus* species also secreted HET-domain containing proteins that have reported involvement in programmed cell death in fungi.³³ These processes may be induced by starvation conditions, consistent with the challenge step in our mycosynthesis process in which carbon and nitrogen sources have been removed. The presence of NAD-/FAD-binding proteins, oxidases, reductases, and dehydrogenases are indicative of oxidative stress, which may be related to the introduction of a metal stress, in this case Zn.³⁴

The number of detected protein fragments does seem to loosely correlate with the particle morphology. In our previous work, *A. niger* (138 protein fragments detected) was shown to produce the coalesced and dissolved morphology every time over eight replicates. *C. cladosporioides* (7 protein fragments detected), formed square plates for 6/8 replicates and the coalesced and dissolving morphology for 2/8 replicates. The three fungi that displayed the ability to form well-defined, spheroid ZnO NPs, *A. versicolor* (7/8 replicates), *P. variotii* (4/8 replicates), and *P. chrysogenum* (4/8 replicates), also produced a middle range of protein fragments in this current study with 53, 43, and 20, respectively.²⁵ These observations suggest that the diversity of the protein profile may possess an optimum range, which in turn influences the nucleation and growth of ZnO NPs. The proteomes of *A. niger* and *A. versicolor* show the greatest overlap (Table S6), despite producing difference ZnO NP morphologies. This observation is not surprising as these fungi are closely related, and further supports the hypothesis that the identity of individual proteins seems to not be essential for the mycosynthesis of ZnO NPs, however, the degree of diversity within the protein profile may play a role in this process.

Nanoscale Page 6 of 22

As previously discussed, it was anticipated that specific proteins are not likely required to produce ZnO NPs, due to the lack of reduction of the Zn metal center in the ZnO lattice. However, the presence and concentration of proteinaceous material in exudates is expected to play an important role in the stabilization of well-defined, spheroid ZnO NPs. Therefore, we measured total protein levels at each stage of our process as follows: (1) after mycelial growth; (2) following mycelial wash with and without Zn challenge, prior to sterile filtration; (3) immediately post sterile filtration; and (4) following the 48-h incubation after sterile filtration with and without the subsequent 2 mM Zn spike. These measurements were performed for both A. versicolor and C. cladosporioides, and each measurement was performed in biological triplicate, except for Stage 3 that was performed in biological duplicate (as the effect of the sterile filtration process was clearly apparent). A three-way analysis of variance (ANOVA) test was performed to probe for statistical differences in protein levels between both fungi, among the three metal introduction conditions (challenged and spiked, no challenge, and no challenge no spike), as well as each stage of the mycosynthesis process. As shown in Table 1, protein levels differed significantly based on the main effects, Fungus and Stage in the mycosynthesis process only, while the Metal Introduction had no effect on protein levels. Further, a significant interaction term was observed between the two main effects (i.e., Fungi and Stage), which overrides the main effect terms. This interaction suggests that the protein level is strongly dependent on the combination of fungal species and the specific stage of the mycosynthesis process.

Table 1 Three-way ANOVA on effects of fungi, metal introduction, and stage on protein level

Source of Variation	Deg. Of Freedom	Sum of Squares	Mean Square	F Statistics	Probability
Main Effects					
Fungus	1	629.953	629.953	34.094	<0.001
Metal Introduction	2	6.684	3.342	0.181	0.835
Stage	3	1769.340	589.780	31.920	<0.001
Two-Way Interactions					
Fungus x Metal Introduction	2	30.167	15.083	0.816	0.449
Fungus x Stage	3	1008.365	336.122	18.191	<0.001
Metal Introduction x Stage	6	80.743	13.457	0.728	0.629
Three-Way Interaction					
Fungus x Metal Intro. x Stage	6	112.936	18.823	1.019	0.426
Residual	42	776.036	18.477		
Total	65	4550.542	70.008		

Additional mean separation analyses (Holm-Sidak method) were performed to elucidate differences in protein levels within these interaction terms (Tables S7- S10). These data suggest that protein levels for *A. versicolor* differ significantly across all stages of the process, except for After filtration (Stage 3) and 48 h Post-Spike (Stage 4; Table S8). Conversely, the protein levels

Page 7 of 22 Nanoscale

for *C. cladosporioides* were similar across all stages in the mycosynthesis process, statistically speaking (Table S9). Given that the metal introduction showed no effect on protein level, we can treat these three trials as biological triplicates and plot them as a single data set (Fig. 1), where the error bars represent the standard error of the mean (SEM) across these replicates. Both fungi displayed reduced protein levels following mycelial growth compared to the protein level present in the PDB growth media $(29.0 \pm 2.3 \text{ ug mL}^{-1}, \text{ mean } \pm \text{ standard deviation})$, suggesting proteinaceous material was consumed during growth by both fungi. Post-growth, *A. versicolor* shows significantly more protein than *C. cladosporioides* (Table S10), which suggests that *C. cladosporioides* consumed more protein during growth than *A. versicolor*, and/or that most of the proteinaceous content within the starting PDB was consumed by both fungi, and the elevated

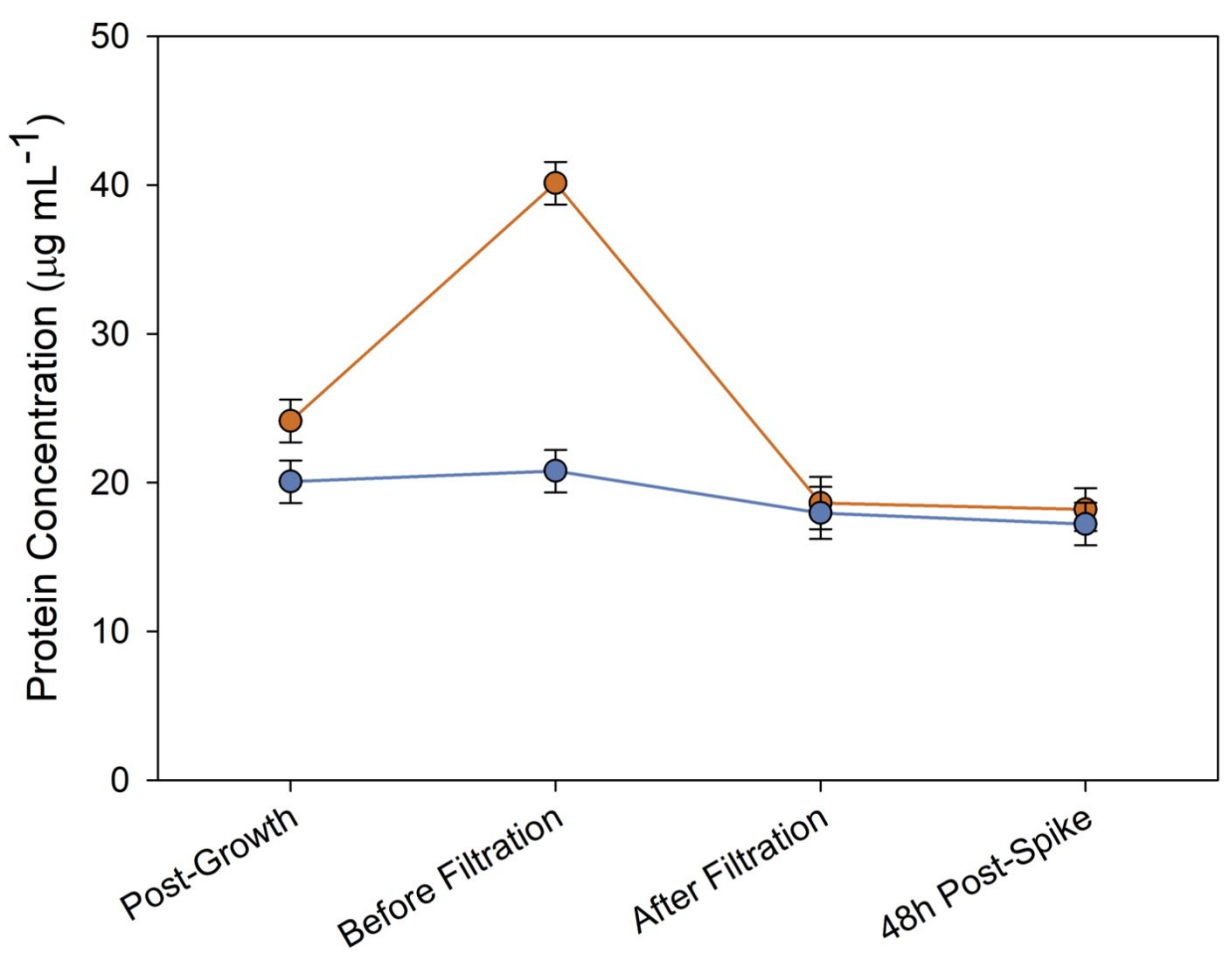


Fig. 1 Protein levels present in exudates of *A. versicolor* (orange) and *C. cladosporioides* (blue) across stages of mycosynthesis process in the production of ZnO NPs.

protein content in *A. versicolor* following growth is due to more secreted protein than *C. cladosporioides*.³⁵ It is likely that both consumption and secretion of proteins are occurring simultaneously and to differing extents, forming the basis for the differences observed between

Nanoscale Page 8 of 22

the two fungi after the growth stage. Under all metal introduction conditions, A. versicolor shows an elevation in protein content following the wash (Stage 2; Fig. 1), with or without Zn challenge, followed by a sharp decline in protein content following sterile filtration (Stage 3, Fig. 1). These data suggest that the induction of a starvation condition, not the metal stress, induces A. versicolor to increase protein production, perhaps to enhance sensing of the environment or in search of food.³⁶ It is important to note here, that these two fungi are fundamentally different in their ecology, with A. versicolor residing in soil and marine environments, breaking down organic material and transporting these nutrients into the hyphae,³⁷ and C. cladosporioides commonly acting as an endophyte residing in plant vasculature, being a known low secreter of biomolecules.³⁵ Interestingly, directly following sterile filtration, the lowest variation in protein levels for both fungi across all conditions is observed, with averages ranging from 18.0 – 18.6 µg/mL protein for A. versicolor and C. cladosporioides, respectively (Fig. 1). These data indicate that both fungal exudates have comparable amounts of soluble protein, but ultimately produce different ZnO NP morphologies, suggesting that these differences are not strictly due to a concentration effect. However, ZnO NP formation was observed at stage 2, following the Zn challenge to the mycelia. It is possible that the elevated level of protein available in the A. versicolor exudate at this stage allows for more colloidally stable ZnO nuclei to form through increased incorporation of protein around the forming NPs. The significant decrease in protein levels observed in A. versicolor after filtration may be due to the inability of proteins associated with the mycelia and spores, such as membrane bound (or anchored) receptors and enzymes, to pass through the membrane filter. It should also be mentioned that the proteomics data previously described were obtained following sterile filtration, so there is a chance, however unlikely, that a specific protein was missed in this qualitative analysis due to complete binding to the filtration membrane. The protein levels remained the same after filtration and 48 h following the subsequent metal spike, despite the differences in the resulting NP morphologies. It should be noted that the protein measured at the final stage after the metal spike may either be free in solution or bound to the surface of ZnO NPs suspended in solution, as this method would not discern between the two populations. Collectively, these data suggest that the levels of proteinaceous material present in exudates likely play a lesser role in the mycosynthesis of ZnO NPs in contrast to the small molecules produced and excreted by these fungi. However, as we will discuss in further detail, the presence of proteinaceous material (not necessarily specific proteins or concentration) may be critical to the formation of well-defined ZnO NPs.

Prior literature suggests that small molecule metabolites excreted by fungi are involved in binding metal ions, ^{17, 38, 39} and likely candidates for regulating the formation of ZnO NPs. Because the metabolomics methodology is ratiometric in nature, the relative abundance of each metabolite was estimated via rank ordering by group area and their prevalence was compared across each fungal exudate. There were 1,159 distinct, named metabolites detected

Page 9 of 22 Nanoscale

across all five fungal exudates. From these, the top 25 metabolites with the greatest peak area from each fungal exudate are shown in Tables S11 – S15. Within these top 25, 53 – 70% of the specific metabolome is covered, and the 25th compound listed accounts for less than 0.65% of the entire metabolome. Therefore, we concluded that comparisons across the top 25 metabolites was sufficient to detail the most prevalent constituents in the fungal exudate involved in ZnO NP formation. From our previous study, we identified *A. versicolor* as the most prominent and robust producer of well-defined, spheroid NPs, whereas *C. cladosporioides* was the fungus most likely to form micro-sized plates. The other three fungi produced highly mixed morphologies including well-defined NPs, highly coalesced/dissolving NPs and/or micron-scale plates. With this in mind, we aimed to identify metabolites that were enriched in the *A. versicolor* exudate compared to the others, with particular attention to *C. cladosporioides*, as a means of ascertaining constituents that were important in forming well-defined NPs. Fig. 2 is a heat map that compares the relative abundance of the top 25 metabolites in *A. versicolor* against the other four fungi, with fold differences

		Ra	Ratio of Metabolite AspV/Fungi X (fold differences)							
		A. niger	· С.	C. cladosprioides		. variotii	P. chrysogenum			
Sulfamic acid		d 1.7		0.4		0.6	0.6			
Hexylamine		ne 0.6		0.6		0.4	0.3			
4-Imidazolemethanol		8.0 lc		1.1		1.3	0.7			
	δ-Valerolactam			4.0		1.8	1.7			
Aminopyrrolnitrin		n 66.9		90.1		13.1	3.3			
Thiamine		ne 11.0		50.7		21.1	2.6			
2'-0	2'-O-Methyladenosine			7.4		0.9	120.3			
O-ureido-D-serine		ne 7.3		21.0		11.7	112.6			
Isovalerylglutamic acid		d 89.2		145.2		597.1	2.3			
Fomepizole		le 7.7		4.9		4.1	1.1			
[Similar to: Thiamine; Δ	[Similar to: Thiamine; Δ Mass: -0.2644 Da]			0.2		0.5	0.5			
L-alpha-Glycerylphosphorylcholine		e 453.8		23.1		5.6	10.8			
Δ		Δ 1.8		0.9		21.6	11.3			
cGMP		IP 416.6		1180.0		0.4	1.0			
Pyrimidine		ne 1.2		0.2		1.7	6.1			
Ω				0.1		546.5	0.1			
Θ		Θ 0.9		0.9		1.0	0.9			
Hexamethylenetetramine		ne 2.6		131.4		1.7	2.4			
Apocynin		n 3.0		0.5		3.9	1.3			
L-Pyroglutamic acid		d 0.2		0.9		1.1	1.1			
Ψ		Ψ 2.5		1.1		1.9	1.1			
Acetylcholine		ne 12.2		34.6		28.4	3.3			
S-(-)-Raclopride		le 7.0		3.4		12.4	1.9			
D-ribosylnicotinate		te 17.1		1.9		1.0	0.4			
Guvacine		ne 1.3		1.3		1.2	2.4			
Legend										
Very Defficient	Defficient	Equivalent	Enric	ched	More Enriched	Very Enrich	ed Most Enriched			
(=0.1)	(0.1-1)	(1±0.1)	(1-	10)	(10 - 100)	(100 - 100	0) (>1000)			

Δ: 1-(1H-Imidazol-5-yl)-3-(phosphonooxy)-2-propanone

Θ: [Similar to: 2-[3-chloro-2-hydroxy-4-methoxy-6-(methoxycarbonyl)phenoxy]-6-hydroxy-4-methylbenzoic acid; ΔMass: -6.7938 Da]

 $[\]Psi$: 4-(2,6-dimethylphenyl)-5-(7-oxabicyclo[2.2.1]hept-2-yl)-2,4-dihydro-3H-1,2,4-triazole-3-thione

 $[\]pmb{\Omega}{:}~5,7-dihydroxy-2-(4-hydroxy-3-methoxyphenyl)-3,4-dihydro-2H-1-benzopyran-4-one$

Nanoscale Page 10 of 22

Fig. 2 Heatmap of top 25 metabolites from *A. versicolor* compared to other fungi tested. Values represented the ratio (fold difference) of a given metabolite observed in *A. versicolor* against that same metabolite observed in the other four fungi.

reported. Here, the higher values represent metabolites whose concentrations are highly enriched in the exudates of *A. versicolor* compared to the other fungi. From these data, the presence of hexamethylenetetramine (HMTA) in the exudate of *A. versicolor*, the 18th most prominent metabolite, was noteworthy for the following reasons. First, HMTA was ~130-fold more concentrated in *A. versicolor* exudate compared to *C. cladosporioides*, and only slightly enriched compared to the other three fungi, which had been observed to synthesize well-defined ZnO NPs at least a portion of the time.²⁵ Second, there are numerous reports of HMTA functioning to bind metal cations and form nanomaterials such as metal organic frameworks in a non-biological context.⁴⁰⁻⁴⁸

As previously described, many reports on the biosynthesis of NPs either challenge the bacteria, fungi, yeast, or leaf extract directly with metal salts, or spike the resulting exudates after the organismal component has been removed.^{21, 39} In our previous work, we challenged the fungus with various Zn salts and subsequently spiked the cell-free exudate with Zn salts as well. We hypothesized that the challenge may stimulate the production and secretion of metabolites necessary to drive interactions with the metal cations and formation of inorganic, crystalline

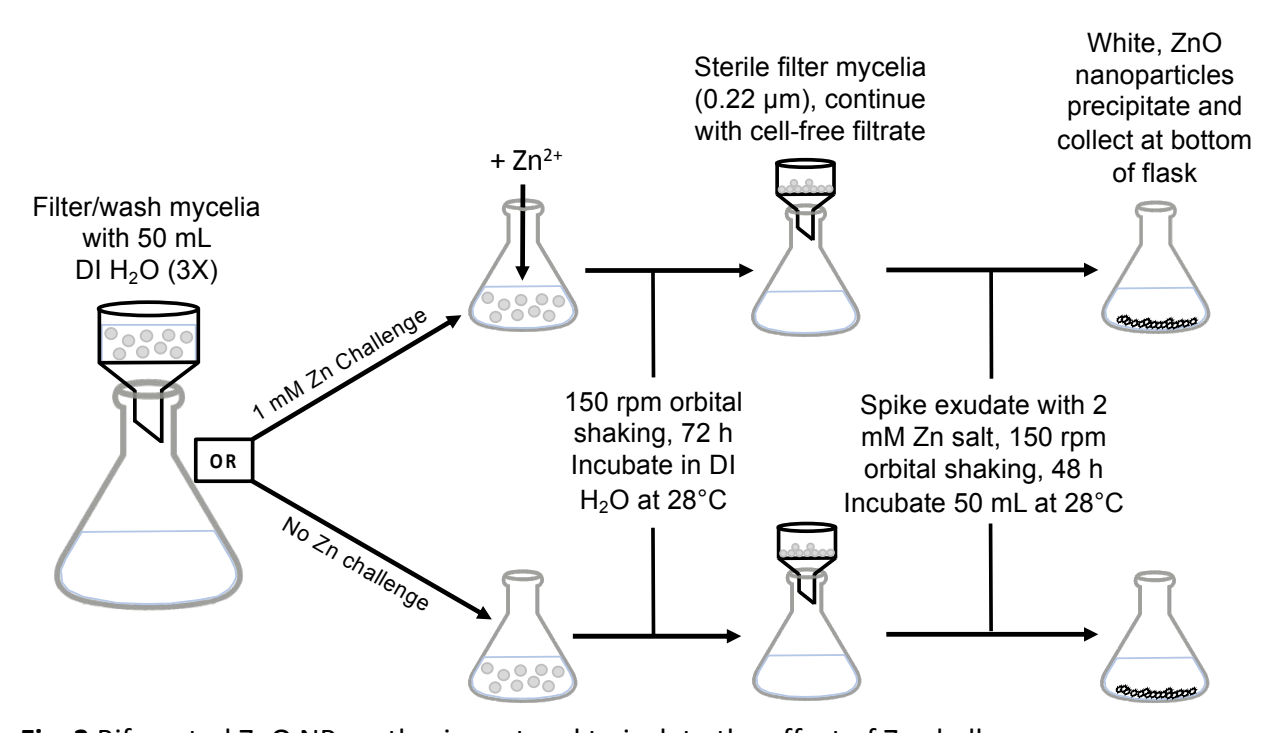


Fig. 3 Bifurcated ZnO NP synthesis protocol to isolate the effect of Zn challenge.

Page 11 of 22 Nanoscale

materials, a process also referred to as biomineralization.²⁵ Here, we bifurcated our original protocol to evaluate the effect of metal challenge on the resulting NP morphology (Fig. 3). In this new approach, we limited the fungi tested to only *A. versicolor* and *C. cladosporioides*, the well-defined NP and plate former, respectively. These fungi were grown as previously described,²⁵ and, following the removal of potato dextrose broth (PDB) growth media, were either challenged with 1 mM ZnCl₂ or not, and incubated at 28 °C with 250 rpm orbital shaking for 72 h. The mycelia were then removed via sterile filtration and the exudate was spiked with an additional 2 mM ZnCl₂. These samples were then incubated for an additional 48 h at the conditions detailed above and drop casted onto carbon backed copper grids for material characterization.

Nanoscale Page 12 of 22

To evaluate changes in the metabolome in the absence of a metal challenge, the exudates of A. from five versicolor biological replicates were collected directly after sterile filtration, without the introduction of Zn salt. Metabolomic analysis discovered 313 compounds present, with HMTA not being detected. The top compounds accounted for 79.7% of the metabolome and are reported in Table S16. These data suggest that the metal challenge does significantly change the profile of small molecules secreted by A. versicolor, including the stimulation of HMTA production. To our knowledge, direct biosynthetic pathway for HMTA have been reported in fungi. However, HMTA may be formed through the spontaneous reaction of formaldehyde and ammonia, two products known to be found in fungal exudates at varying levels.49-51 Intracellular formaldehyde levels in

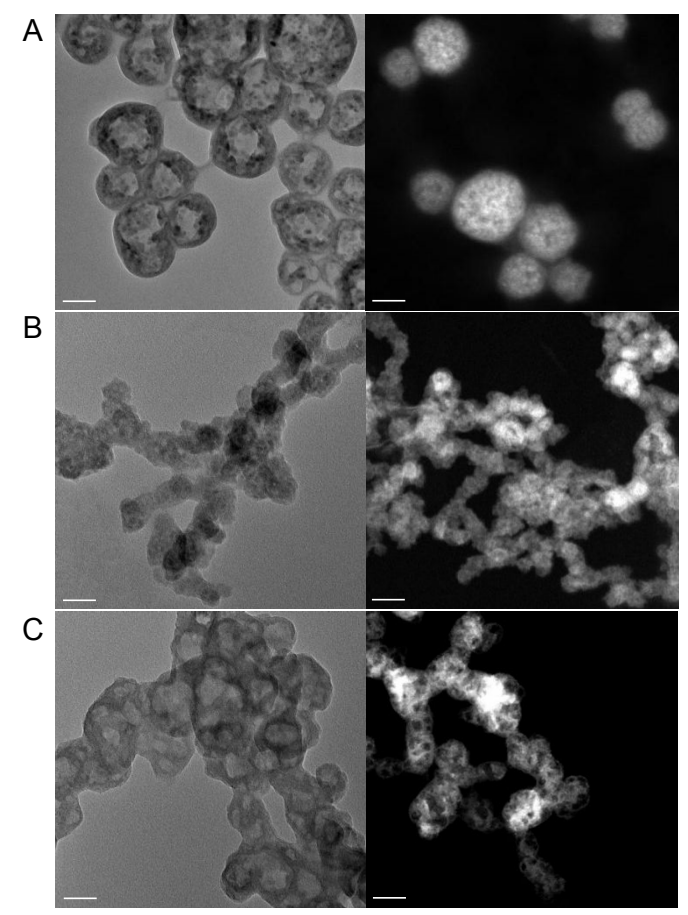


Fig. 4 TEM (left) and HAADF-STEM (right) images of ZnO particles synthesized using a challenged *A. versicolor* exudate (A), HMTA non-biological control (B), and unchallenged *A. versicolor* exudate (C). Scale bars are 50 nm.

certain Basidiomycetes have been shown to spike ~20 h following environmental stress such as metal challenge or increased temperature.⁵² Likewise, ammonia production by certain fungi, including *A. fumigatus*, has been shown to increase in the presence of low amounts of amino acids.⁵³ In the present study, both the metal stress and carbon/nitrogen starvation conditions are present following the wash of the mycelia and reconstitution in distilled water. Collectively, these conditions are consistent with those reported to produce ammonia and formaldehyde, which may in turn have enabled the formation of HMTA and subsequent mycosynthesis of ZnO NPs.

The effects of metal challenge and carbon/nitrogen starvation were then determined, separately, with respect to the resulting morphology of ZnO NPs. We characterized the nanostructures formed from the following three conditions: (1) challenged *A. versicolor* exudate containing HMTA, (2) unchallenged *A. versicolor* exudate lacking HMTA, and (3) a non-

Page 13 of 22 Nanoscale

biological control containing only HMTA and Zn salt. For the non-biological control, Zn and HMTA were added in a 1:20 molar ratio (1 mM Zn to 20 mM HMTA), as this ratio has previously been reported to produce ZnO NPs.⁴⁴ Ratios as low as 0.1 to 20 and up to 5:20 Zn to HMTA did not produce ZnO NPs (data not shown).

As previously described, the proteinaceous materials surrounding mycosynthesized ZnO NPs confound diffraction traditional X-ray analysis, conveying the need for more targeting diffraction techniques to check crystallinity.²⁵ All conditions described in Fig. 4 produced crystalline material as evidenced by electron diffraction (Fig. S1), which contain d- spacings consistent with the hexagonal or Wurtzite confirmation of ZnO (ICDD#: 00-036-1451). transmission electron microscopy (TEM, Left) and high angle annular darkfield scanning transmission electron microscopy (HDAAF-STEM, Right), illuminated nuances in the greater structures produced from these different conditions (Fig. 4). Fig. 4A shows the well-defined, spheroid ZnO NPs that were observed previously, arising from challenged and spiked A. versicolor. In Fig. 4B, the non-biological HMTA and Zn control, a more mesh-like structure was observed, where dense metal clusters are present, but the border region has become completely coalesced, possibly due to the lack of proteinaceous material to prevent further coagulation. These non-biological HMTA and Zn control samples were drop casted 48 h after the sterile filtration and

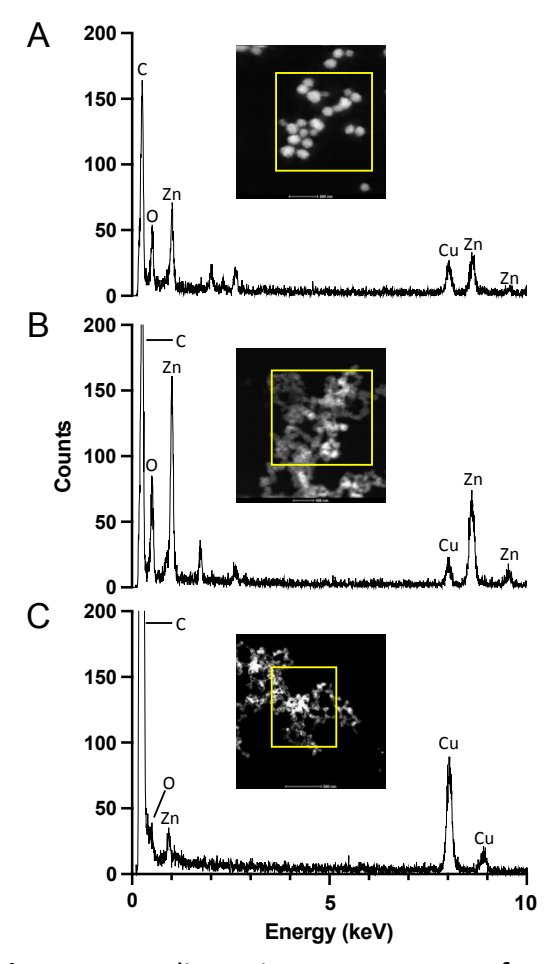


Fig. 5 Energy dispersive X-ray spectra of ZnO NPs made from challenged *A. versicolor* exudate (A), HMTA and Zn non-biological control (B), and unchallenged *A. versicolor* exudate (C). HAADF-STEM images of each sample are shown (inset) with a yellow box outlining the area analyzed to produce each spectrum.

spike, as described in Fig. 3. When these samples were left at room temperature for one week and drop-casted onto TEM grids, the observed mesh-like structure was lost, and fully coagulated micro-sized structures were obtained (Fig. S2). This observation supports the hypothesis that without protein present to form a protein corona, the structures continue to

Nanoscale Page 14 of 22

coagulate over time. Interestingly, in the unchallenged condition (Fig. 4C), hollow nanotubular structures are obtained, suggesting that without the HMTA to act as a metal chelator, the Zn nanostructures become less dense. All these nanomaterials were confirmed to contain primarily Zn and O by energy dispersive X-ray spectroscopy (EDS; Fig. 5).

Fourier transform infrared spectroscopy (FTIR) shows distinct differences in the ZnO NPs formed from A. versicolor and C. cladosporioides exudates, as well as the HMTA non-biological control (Fig. 6). The non-biological control (Fig. 6, blue trace) correlates well with the previously published spectrum for HMTA.⁴¹ The HMTA peak at 1006 cm⁻¹ broadening and shifting to 1050 cm⁻¹ following incorporation into a Zn-containing NP lattice is also in line with the literature and our previous findings.^{25, 41} Being that HMTA was not observed in the metabolome of unchallenged A. versicolor exudate, these findings suggest that this broad peak at 1050 cm⁻¹ is likely due to an amide stretch (N-H), as previously reported,²⁵ swamping out the HMTA signal in the case of challenged A. versicolor exudate. The FTIR spectrum for C. cladosporioides lacks significant signals in this HMTA and amide stretch position, indicating the absence of HMTA or large amounts of proteinaceous material, as we would expect. These data further support the hypothesis that the lower surface area, plate morphology of ZnO produced by C. cladosporioides, incorporate fewer proteinaceous capping agents around the nanostructure, as compared to ZnO NPs produced by A. versicolor exudate. As previously mentioned, this may be due to more protein being present in the A. versicolor exudate following the Zn challenge, leading to greater incorporation around the forming ZnO NPs.

Conclusions

Overall, our data suggest that the secretion of small molecule metabolites, and not proteins, in fungal exudates is the primary regulator of the resulting ZnO NP morphology. In particular, the presence of metal chelators such as HMTA in fungal exudates are likely critical to the production of dense, welldefined ZnO NPs potentially facilitating nucleation of the metal centers into the ZnO lattice. Moreover, the differences in the metabolomes due to Zn challenge suggest that enhanced production and secretion of small molecules due to a Zn stress is critical to

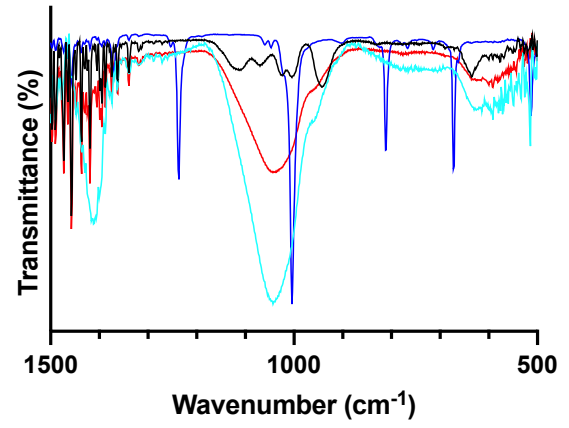


Fig. 6 FTIR of ZnO NPs formed from *A. versicolor* exudate following Zn challenge (cyan), without Zn challenge (red), *C. cladosporioides* following Zn challenge (black), and non-biological control containing HMTA and Zn (blue).

the formation of well-defined ZnO NPs. In contrast, the composition and concentration of

Page 15 of 22 Nanoscale

proteinaceous material in fungal exudates did not correlate with differences in the NP morphologies. The secreted proteins, however, may play a role in forming a corona around the well-defined ZnO NPs, preventing coagulation into larger micro-sized structures. Collectively, these results provide a deeper, more comprehensive understanding of the biochemical factors that are critical to mycosynthesis, which in turn may be leveraged to regulate the size and shape of NPs in future studies. These mechanistic insights will permit more control over this biologically derived process, allowing for more cost-effective and environmentally benign ZnO NP synthesis for specific applications. Because mycosynthesized ZnO NPs exhibit a typical Wurtzite structure, we expect these NPs will share similar properties and associated application space, including their use as antimicrobials and photoelectric/photocatalytic materials. More focused studies on functional properties, however, are necessary to determine what effect, if any, the protein corona has on performance in these varied applications.

Author Contributions

N.B. conceptualized experiments, prepared all samples for this work, performed FTIR and brightfield TEM (Fig. S2), assisted in data analysis, and wrote the manuscript. S.O. assisted N.B. in sample preparation and conceptualization. W.K. performed TEM and HAADF-STEM (Fig. 4), EDS (Fig. 5), and CBED (Fig. S1). B.B. and P.M. performed proteomics (Tables S1-S5) and metabolomics (Fig. 2, Tables S11-S16). J.W. assisted N.B. in Brightfield TEM (Fig. S2) and interpretation of electron microscopy results. G.B. assisted N.B. in conceptualization of experiments, interpretation of results, and performed statistical analysis (Table 1, Fig. 1, Tables S7-S10). N.B wrote the original draft, and all authors contributed to the critical review and editing of this manuscript.

Experimental

Fungus cultivation

Environmental isolates of *A. niger, A. versicolor, C. cladosporioides, P. variotti,* and *P. chrysogenum* were used for metabolomic and proteomic characterization based on their previously demonstrated abilities to synthesize ZnO nanostructures, and were cultivated as previously described.²⁵ Briefly, potato dextrose agar plate (PDA) was inoculated by placing a 5 mm mycelia/PDA plug mycelia side down in the center of the plate (the plug was transferred via flame sterilized, glass transfer pipet). The freshly inoculated plate was incubated at 25°C for at least 72 h prior to further use. After incubation, three plugs 5 mm in diameter were excised from the growing edge of the mycelia and placed into a 250 mL Erlenmeyer flask containing 100 mL of autoclaved-sterile PDB media (pH ~5) and incubated for 72 h at 28°C with 150 rpm orbital shaking. The PDB was then removed through a Whatman No. 1 Filter under vacuum, and the mycelia was washed with DI water three times. The washed mycelia were then resuspended in

Nanoscale Page 16 of 22

deionized water, treated with the appropriate metal challenge condition to be tested, and incubated at 28 °C with 150 rpm orbital shaking for 72 h. The pH of the resulting media was neutral, ranging from $^{\sim}6.4 - 7.2$, as previously described. ²⁵

Nanoparticle biosynthesis

For synthesis trials containing a Zn challenge, mycelia of *A. versicolor* and *C. cladosporioides* were placed in a 125 mL Erlenmeyer flask containing deionized water (50 mL) with $ZnCl_2$ (1 mM). For trials excluding the metal challenge, mycelia were placed in a 125 mL Erlenmeyer flask containing DI water (50 mL) only. Both challenged and unchallenged flasks were incubated at 28 °C with 150 rpm orbital shaking for 72 h. After the incubation period, the mycelia were removed from exudate via sterile filtration using a 0.22 μ m filter under vacuum. The fungal exudate (filtrate) was then transferred to a 125 mL Erlenmeyer flask, and the mycelia were discarded. The flask was then spiked with additional $ZnCl_2$ (2 mM), which was added to both challenged and unchallenged samples (except for the metabolomics/proteomics sample, which was taken following sterile filtration, but before the subsequent 2 mM spike of Zn metal). The spiked exudate was then incubated for 48 h at 28 °C with 150 rpm orbital shaking (Fig. 3).

Proteomics sample preparation

A Pierce[™] BCA Protein Assay Kit (Thermo Fisher Scientific, Cat. # 23227) was used according to manufacturer's protocol, to determine protein content. Samples were then normalized to a consistent protein concentration by dilution with LC-MS grade water (Thermo Scientific, Cat.# 047146.M6) prior to further processing. Proteins (100 ug total protein) were extracted and digested using S-Trap micro columns (Protifi, Cat. # CO2-micro-80) according to the manufacturer's protocol but replacing 120 mM TCEP and 500 mM MMTS with 20 mM DTT and 40 mM IAA, respectively. Mass spectrometry-grade Trypsin/Lyc-C mix (Promega, Cat. # V5072) was used for digestion with an overnight incubation. Final extracts were evaporated to dryness in a SpeedVac vacuum concentrator (Labconco) and reconstituted in LC-MS grade water with 0.1% formic acid to a final protein concentration of 1.0 μg/μL.

Proteomics data acquisition

LC-MS analysis was performed on a U3000 nano-LC system paired with an Eclipse Tribrid mass spectrometer with an EASY-spray ion source (Thermo Fisher Scientific, San Jose, CA, USA). A 4 μ L injection was separated on an EASYspray c18 column (75 cm x 75 μ m, Thermo Scientific, Cat. # ES75750PN) over a 65-minute gradient at a flow rate of 250 nL/min. Mobile phase A consisted of water with 0.1% formic acid and mobile phase B of acetonitrile with 0.1% formic acid. The LC gradient was 0-3.32 min: 5-10% B, 3.32-49.8 min: 10-35% B, 49.8-52.4 min: 35-70% B, 52.4-53.6 min: 70-90% B, 53.6-56.8 min: 90% hold B, 56.8-57.3 min: 90-5% B, 57.3-65.0 min: 5% hold B. Mass spectrometric data was acquired using data-dependent acquisition at 3s time cycles. Full

scan spectra were collected at 240,000 resolution over a range of 375 to 1500 m/z. The top 20 most abundant monoisotopic peaks detected in each full scan were isolated for MS2 analysis using a normalized collision energy of 30. Only peptides with charge states 2–6 were selected for fragmentation, and product ions were analyzed on the ion trap using the turbo scan setting.

Nanoscale

Proteomics data processing

Protein assignments from the resulting spectra were determined with Proteome Discoverer 3.0. FASTA files were generated by downloading all sequences from UnitProt, related to the specific species in question.

Metabolomics sample preparation

Metabolites in fungal exudates were isolated with a protein precipitation method prior to analysis by LC-MS. Briefly, a 100 μ L aliquot was combined with 400 μ L crash solvent (8:1:1 acetonitrile:methanol:acetone, v/v/v), vortexed, then placed at 4° C for 30 mins to further precipitate proteins. Solutions were then centrifuged at 20,000 g for 10 mins to pellet proteins. A 450 μ L aliquot of the resulting supernatant was transferred to a clean microcentrifuge tube and evaporated to dryness using a SpeedVac vacuum concentrator. Samples were reconstituted in 100 μ L LC-MS grade water with 0.1% formic acid, vortexed briefly, then placed at 4° C for 10 mins. This final solution was again centrifuged at 20,000 g for 10 and the supernatant transferred to a glass, low-volume autosampler vial (Agilent Technologies).

Metabolomics data acquisition

Samples of each fungal exudate were analyzed in technical triplicate on a Thermo Fisher U3000 LC coupled to a 480 Exploris orbitrap mass spectrometer. A 4 μ L injection was separated under gradient flow at 350 μ L/min on a Waters Cortecs T3 column (150 x 2.1 mm, 1.8 μ m). Mobile phase A was LC-MS grade water with 0.1% formic acid and mobile phase B was LC-MS grade acetonitrile with 0.1% formic acid. The gradient was 2% B for the first 3 minutes, increased to 5% B from minute 3 to 8 min, 35% B at 12 min, 95% B at 15 min, held for 3 min, then reequilibrated for 4 min at 2% B. Samples were acquired in positive ionization mode with a heated electrospray ionization source at 3500 V, sheath gas 50 (arbitrary units), auxiliary gas 10 (arbitrary units), sweep gas 1 (arbitrary units), ion transfer tube at 325° C, and vaporizer temperature at 350 °C. Data were acquired in data dependent acquisition mode with the top 20 highest abundance precursor ions isolated for MS2. Full scans were acquired at 120,000 resolution over a scan range of 70-700 m/z, and MS2 fragmentation at normalized HCD energy of 20, 50, 100 acquired at 15,000 resolution.

Metabolomics data processing

Nanoscale Page 18 of 22

Acquired data were processed using Compound Discoverer v3.3 (Thermo Scientific) using an untargeted metabolomic workflow. Blanks were utilized for background identification, and compounds were identified from MS1 or MS2 library search using the mzCloud database, Chemspider database (BioCyc, KEGG, HMDB).

Nonbiological nanoparticle synthesis

Non-biological samples were prepared by adding hexamethylenetetramine (HMTA, 20 mM) and ZnCl₂ (1mM) to DI water (10 mL) in a 20 mL scintillation vial. The solution was vortexed after all constituents were added and stored at room temperature for 24 h without agitation prior to drop casting onto TEM grid.

TEM sample preparation

After the final 48 h incubation (Fig. 3), 10 mL of all biological samples were decanted into a 20 mL scintillation vial and left to rest at room temperature for 24 h without agitation to let the nanoparticles precipitate. After the 24 h period, the scintillation vial was sonicated for 10 min, a 5 μ L aliquot was taken from the sample and placed on a carbon backed 300 mesh copper grid (Ted Pella, Inc. Product #: 0 1843 – F), and dried under air for 10 min. The copper grids were then washed 3 times with 5 μ L aliquots of 100% ethanol, using a Kimwipe to remove organics and excess ethanol from the grid. The samples were then imaged using a ThermoFisher Scientific Talos L120C transmission electron microscope, operating at 120 kV.

TEM/STEM/CBED/XEDS

Transmission electron microscopy (TEM), scanning transmission electron microscopy (STEM), convergent beam electron diffraction (CBED), and energy dispersive X-ray spectroscopy (XEDS) analysis was performed using a Tecnai F30 TEM operating at 300 keV equipped with an EDAX XEDS detector.

Fourier transform infrared spectroscopy

FTIR measurements were obtained using a Shimadzu IRSpirit spectrometer, using a QATR-S single reflection attenuated total reflection (ATR) assembly. Two consecutive 5 μ L aliquots of sample (10 μ L total) were dried onto the ATR crystal under air for 15 min per aliquot. The spectra were baseline and atmosphere corrected using LabSolutions IR software included with the spectrophotometer. Spectra were normalized to the minimum transmittance value for ease of comparison on a single Y-axis.

Quant-iT[™] Protein Assay

One mL aliquots were taken at various stages: (1) from the PDB solution directly after mycelial growth phase, (2) following the 72-h incubation period after challenge, and (3) after the 48-h

Page 19 of 22 Nanoscale

incubation period following sterile filtration and Zn spike. This sampling method was adhered to for both *A. versicolor* and *C. cladosporioides* samples. The protein assay used in this experiment was a Quant-iT TM Protein assay kit by Life Technologies (Thermo-Fisher Scientific, Catalog no. Q33210) was used to measure protein levels at each of the stages listed above. In this assay, a calibration curve was performed using standards ranging from 0-500 ng protein, which added in triplicate in a 96-well plate. $20~\mu$ L and $50~\mu$ L aliquots of fungal exudate were then added to separate wells on the same plate. A Quant-iT TM working solution was made by diluting the Quant-iT TM protein reagent (fluorescent dye) in Quant-iT TM buffer solution at a 1:200 ratio. Once all protein standards and fungal exudates were added to the plate, $200~\mu$ L of the Quant-iT TM working solution was added to each well and mixed by multi-channel micropipette. The plate was then covered with aluminum foil to ensure light bleaching would not affect fluorescence results and incubated at room temperature for 15 min. The plate was then placed into a PerkinElmer, Wallac 1420 Multilabel Counter microplate reader to measure fluorescence emission. The spectrophotometer was configured with excitation and emission wavelengths of 470 nm and 570 nm, respectively, with a 1 s integration time.

Conflict of interest

There are no conflicts to declare.

Acknowledgements

We would like to thank Charlie Easterling for critically reviewing this manuscript. This work was performed, in part, at the Center for Integrated Nanotechnologies, an Office of Science User Facility operated for the U.S. Department of Energy (DOE) Office of Science. Sandia National Laboratories is a multimission laboratory managed and operated by National Technology & Engineering Solutions of Sandia, LLC, a wholly owned subsidiary of Honeywell International, Inc., for the U.S. DOE's National Nuclear Security Administration under contract DE-NA-0003525. The views expressed in the article do not necessarily represent the views of the U.S. DOE or the United States Government. Los Alamos National Laboratory, an affirmative action equal opportunity employer, is managed by Triad National Security, LLC for the U.S. Department of Energy's NNSA, under contract 89233218CNA000001.

Nanoscale Page 20 of 22

Works Cited

- 1. M. Premanathan, K. Karthikeyan, K. Jeyasubramanian and G. Manivannan, *Nanomedicine: Nanotechnology, Biology and Medicine* 2011, 7 (2), 184-192.
- 2. O. Maťátková, J. Michailidu, A. Miškovská, I. Kolouchová, J. Masák and A. Čejková, *Biotechnology Advances* 2022, *58*, 107905.
- 3. P. K. Dikshit, J. Kumar, A. K. Das, S. Sadhu, S. Sharma, S. Singh, P. K. Gupta and B. S. Kim, *Catalysts* 2021, *11* (8), 902.
- 4. H. Bouzid, M. Faisal, F. A. Harraz, S. A. Al-Sayari and A. A. Ismail, *Catalysis Today* 2015, *252*, 20-26.
- 5. C. Dias, M. Ayyanar, S. Amalraj, P. Khanal, S. Vijayakumar, S. Das, P. Gandhale, V. Biswa, R. Ali, N. Gurav, S. Nadaf, N. Rarokar and S. Gurav, *Journal of Drug Delivery Science and Technology* 2022, 103444.
- 6. X. Ma and X. Wang, Plant Exposure to Engineered Nanoparticles, 2022; **3**, pp 195-207.
- 7. N. Jain, A. Bhargava, S. Majumdar, J. Tarafdar and J. Panwar, *Nanoscale* 2011, **3** (2), 635-641.
- 8. V. V. Kadam, J. P. Ettiyappan and R. M. Balakrishnan, *Materials Science and Engineering: B* 2019, **243**, 214-221.
- 9. J. Sarkar, M. Ghosh, A. Mukherjee, D. Chattopadhyay and K. Acharya, *Bioprocess Biosyst Eng* 2014, **37** (2), 165-71.
- 10. A. Gade and M. Rai, *Mycology: Biology and Biotechnological Applications*, 2021; pp 245-262.
- 11. A. Es-haghi, M. E. Taghavizadeh Yazdi, M. Sharifalhoseini, M. Baghani, E. Yousefi, A. Rahdar and F. Baino, *Biomimetics* 2021, 6 (2), 34.
- 12. S. Chatterjee, S. Mahanty, P. Das, P. Chaudhuri and S. Das, *Chemical Engineering Journal* 2020, *385*, 123790.
- 13. Z. Qin, Q. Yue, Y. Liang, J. Zhang, L. Zhou, O. B. Hidalgo and X. Liu, *Journal of Biotechnology* 2018, **284**, 52-56.
- 14. A. S. Vijayanandan and R. M. Balakrishnan, *Journal of Environmental Management* 2018, **218**, 442-450.
- 15. N. I. Hulkoti and T. C. Taranath, Colloids and Surfaces B: Biointerfaces 2014, 121, 474-483.
- 16. R. Mahendra, G. Indarchand, B. Shital, I. Pramod, S. Sudhir, G. Swapnil, R. A. Mehdi and G. Aniket, *The Genus Aspergillus*, 2022; p Ch. 6.
- 17. G. M. Gadd, Microbiology 2010, 156 (3), 609-643.
- 18. S. Ghosh, R. Ahmad, M. Zeyaullah and S. K. Khare, Frontiers in Chemistry 2021, 9.
- 19. M. Kitching, M. Ramani and E. Marsili, Microb Biotechnol 2015, 8 (6), 904-17.
- 20. P. Ingle, K. Kamble, P. Golińska, M. Rai and A. Gade, *Mycosynthesis of Nanomaterials*, CRC Press: pp 233-253.
- 21. K. S. Siddigi and A. Husen, Nanoscale Research Letters 2016, 11 (1), 98.
- 22. M. Sastry, A. Ahmad, M. I. Khan and R. Kumar, Current Science 2003, 85 (2), 162-170.
- 23. A. Ahmad, P. Mukherjee, S. Senapati, D. Mandal, M. I. Khan, R. Kumar and M. Sastry, *Colloids and surfaces B: Biointerfaces* 2003, *28* (4), 313-318.
- 24. V. Bansal, P. Poddar, A. Ahmad and M. Sastry, *Journal of the American Chemical Society* 2006, **128** (36), 11958-11963.

Page 21 of 22 Nanoscale

- 25. N. G. Brady, S. L. O'Leary, G. C. Moormann, M. K. Singh, J. Watt and G. D. Bachand, *Small* 2023, *19* (15), 2205799.
- 26. M. Harpke, S. Pietschmann, N. Ueberschaar, T. Krüger, O. Kniemeyer, A. A. Brakhage, S. Nietzsche and E. Kothe, *Genes (Basel)* 2022, *13* (9).
- 27. Y. Dachuan and Q. Jinyu, *PeerJ* 2021, **9**, e11115.
- 28. N. Durán, P. D. Marcato, O. L. Alves, G. I. H. De Souza and E. Esposito, *Journal of Nanobiotechnology* 2005, **3** (1), 8.
- 29. N. Jain, A. Bhargava, J. C. Tarafdar, S. K. Singh and J. Panwar, *Applied Microbiology and Biotechnology* 2013, **97** (2), 859-869.
- 30. R. Marmorstein, M. Carey, M. Ptashne and S. C. Harrison, *Nature* 1992, *356* (6368), 408-414.
- 31. T. Pan and J. E. Coleman, *Proc Natl Acad Sci U S A* 1990, **87** (6), 2077-81.
- 32. S. MacPherson, M. Larochelle and B. Turcotte, *Microbiol Mol Biol Rev* 2006, **70** (3), 583-604.
- 33. M. Paoletti, C. Clavé and *Eukaryot Cell* 2007, **6** (11), 2001-8.
- 34. Y. Teng, X. Du, T. Wang, C. Mi, H. Yu, L. Zou and *Archives of Microbiology* 2018, **200** (1), 159-169.
- 35. K. Bensch,; U. Braun, J. Z. Groenewald and P. W. Crous, *Studies in Mycology* 2012, **72**, 1-401.
- 36. B. M. Nitsche, T. R. Jørgensen, M. Akeroyd, V. Meyer and A. F. Ram, *BMC Genomics* 2012, 13, 380.
- 37. M. Piontek, K. Łuszczyńska and H. Lechów, Int J Environ Res Public Health 2016, 13 (9).
- 38. M. Fomina, S. Hillier, J. Charnock, K. Melville, I. J. Alexander and G. Gadd, *Applied and Environmental Microbiology* 2005, **71** (1), 371-381.
- 39. J. Singh, T. Dutta, K. H. Kim, M. Rawat, P. Samddar and P. Kumar, *Journal of nanobiotechnology* 2018, *16* (1), 1-24.
- 40. R. Parize, J. Garnier, O. Chaix-Pluchery, C. Verrier, E. Appert and V. Consonni *The Journal of Physical Chemistry C* 2016, **120** (9), 5242-5250.
- 41. K. Vijai Anand, R. Mohan, R. Mohan Kumar, M. Karl Chinnu and R. Jayavel, *Journal of Experimental Nanoscience* 2014, *9* (3), 261-271.
- 42. X. Qiao, Y. Ge, Y. Li, Y. Niu and B. Wu, ACS Omega 2019, 4 (7), 12402-12409.
- 43. M. Fterich, F. B. Nasr, R. Lefi, M. Toumi and S. Guermazi, *Materials Science in Semiconductor Processing* 2016, *43*, 114-122.
- 44. N. Salah, W. M. Al-Shawafi, S. S. Habib, A. Azam and A. Alshahrie, *Materials & Design* 2016, **103**, 339-347.
- 45. D. Jesuvathy Sornalatha and P. Murugakoothan, Materials Letters 2014, 124, 219-222.
- 46. H. Avireddy, H. Kannan, P. Shankar, G. K. Mani, A. J. Kulandaisamy and J. B. B. Rayappan, *Materials Chemistry and Physics* 2018, **212**, 394-402.
- 47. A. Saranya, T. Devasena, H. Sivaram, R. Jayavel and *Materials Science in Semiconductor Processing* 2019, *92*, 108-115.
- 48. P. Y. Wu, J. Pike, F. Zhang and S. W. Chan, *International Journal of Applied Ceramic Technology* 2006, *3* (4), 272-278.
- 49. R. K. Wood, W. F. Stevens, Journal of Applied Chemistry 1964, 14 (8), 325-330.

- 50. A. T. Nielsen, D. W. Moore, M. D. Ogan, R. L. Atkins and *The journal of organic chemistry* 1979, *44* (10), 1678-1684.
- 51. Y. Ogata, A. Kawasaki, Bulletin of the Chemical Society of Japan 1964, 37 (4), 514-519.
- 52. A. Jarosz-Wilkolazka, M. Fink-Boots, E. Malarczyk and A. Leonowicz, *Acta biologica Hungarica* 1998, *49*, 393-403.
- 53. R. J. St Leger, J. O. Nelson and S. E. Screen, *Microbiology (Reading)* 1999, **145** (*Pt 10*), 2691-9.